Inorganic Chemistry

ARTICLE

pubs.acs.org/IC

Electrochemistry and Spectroelectrochemistry of Bismanganese Porphyrin-Corrole Dyads

Ping Chen,[†] Maya El Ojaimi,[†,‡] Claude P. Gros,[‡] Philippe Richard,[‡] Jean-Michel Barbe,[*,‡] Roger Guilard,[‡] Jing Shen,[†] and Karl M. Kadish[*,†]

[†]Department of Chemistry, University of Houston, Houston, Texas 77204-5003, United States

[‡]Université de Bourgogne, ICMUB (UMR 5260), 9 Avenue Alain Savary BP 47870, 21078 Dijon Cedex, France

Supporting Information

ABSTRACT: A series of homobimetallic manganese cofacial porphyrin-corrole dyads were synthesized and investigated as to their electrochemistry, spectroelectrochemistry, and ligand binding properties in nonaqueous media. Four dyads were investigated, each of which contained a Mn(III) corrole linked in a face-to-face arrangement with a Mn(III) porphyrin. The main difference between compounds in the series is the type of spacer, 9,9-dimethylxanthene, anthracene, dibenzofuran, or diphenylether, which determines the distance and interaction between the metallomacrocycles. Each redox process of the porphyrin-corrole dyads was assigned on the basis of spectroscopic and electrochemical data and by comparison with reactions and properties of the monocorrole and the monoporphyrin which were examined under the same solution conditions. The Mn(III) porphyrin part of the dyad undergoes two major one-electron reductions in pyridine and benzonitrile, the first of which involves a Mn(III)/Mn(II) process and the second the addition of an electron to the conjugated π-ring system of the macrocycle. The Mn(III) corrole part of the dyads also exhibits two major redox processes, one involving Mn(III)/Mn(II) and the other Mn(III) to Mn(IV) under the same solution conditions. The potentials and reversibility of each electron transfer reaction were shown to depend upon the solvent, type of spacer separating the two macrocycles, and the presence or absence of axial ligation, the latter of which was investigated in detail for the case of acetate ion which was found to bind within the cavity of the dyad to both manganese centers, both before and after the stepwise electroreduction to the Mn(II) forms of the two macrocycles. An intramolecular chloride ion exchange between the porphyrin part of the dyads which contain $Mn^{III}Cl$ and the singly oxidized corrole in the dyad is observed after the Mn(III)/Mn(IV) reaction of the corrole, suggesting that chloride is coordinated inside the cavity in the neutral compound.

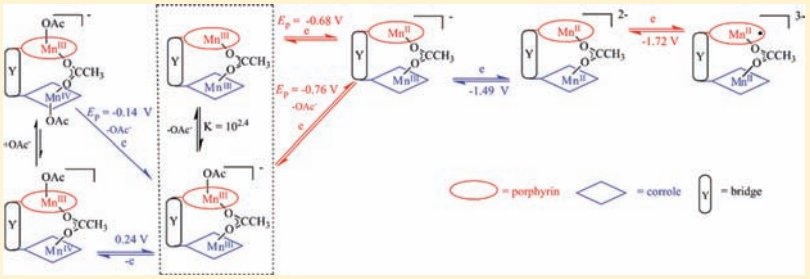

INTRODUCTION

Pacman-type metallo-bisporphyrinoïd systems have been used as catalysts for many oxidation reactions.[1−8] These dyads consist of two macrocycle linked in a face-to-face (cofacial) arrangement by a "rigid" or "flexible" bridge to encapsulate guest molecules inside the bismacrocycle pocket, with the exact stoichiometry depending upon the specific combination of metal ions, solvent, and shape or length of the bridging spacer.[9−14] Changes in the bridge structure have been used to control the distance between the two porphyrin moieties in the dyad as well as the degree of opening and closing which is directly related to changes in the extent of $\pi-\pi$ interaction between the two macrocycles and the overall properties of the compound.[15−19]

Our own interest in this area has focused in large part on biscorroles, bisporphyrins, and porphyrin-corrole dyads containing manganese or cobalt as central metals,[1,2,11,12,20−24] each of which can exist in both high and low oxidation states and with different degrees of axial ligation under the application of a preselected oxidizing or reducing potential. We recently reported how anion and solvent binding will affect redox potentials and axial ligation of monomeric Mn(III) corroles[8] and now turn our attention to the electrochemistry, spectroelectrochemistry, and ligand binding properties of four dyads containing the same metallocorrole, (Mes_2PhCor)Mn (**1**), linked in a face-to-face arrangement with a second Mn(III) porphyrin, the main difference between compounds in the series being the type of spacer which determines the distance and interaction between the two metallomacrocycles. The investigated bis-manganese porphyrin-corrole dyads (**3**−**6**) are shown in Chart 1. Also included for comparison with these bismacrocycles are the related manganese monocorrole **1** and monoporphyrin **2**, the first of which whose electrochemistry has already been described in the literature.[25] The same linking bridges as in past studies were used in the

Received: December 1, 2010
Published: March 15, 2011

Chart 1. Structures of Investigated Bis-manganese Complexes

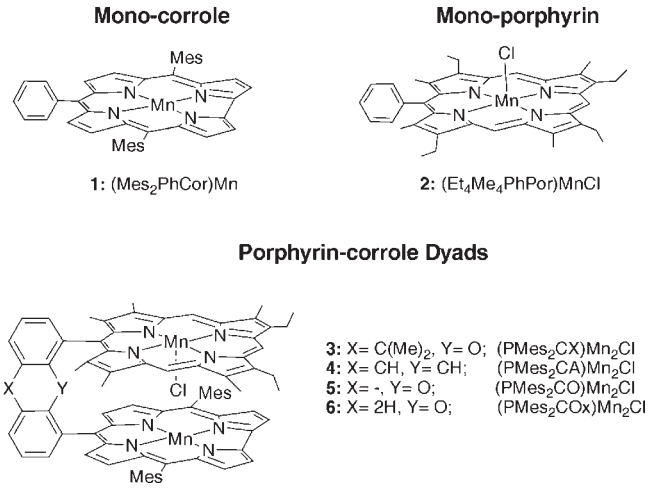

current investigation, 9,9-dimethylxanthene (X), anthracenyl (A), dibenzofuran (O), and diphenylether (Ox). The dyads in Chart 1 as well as other related high valent manganese porphyrins and corroles are of interest with respect to their properties as oxidation catalysts.[26−37]

EXPERIMENTAL SECTION

Instrumentation. Cyclic voltammetry was carried out with an EG&G model 173 potentiostat/galvanostat. A homemade three-electrode electrochemistry cell was used and consisted of a platinum button or glassy carbon working electrode, a platinum wire counter electrode, and a saturated calomel reference electrode (SCE). The SCE was separated from the bulk of the solution by a fritted-glass bridge of low porosity which contained the solvent/supporting electrolyte mixture. All potentials are referenced to the SCE.

UV−visible spectroelectrochemical experiments were performed with an optically transparent platinum thin-layer electrode of the type described in the literature.[38] Potentials were applied with an EG&G Model 173 potentiostat/galvanostat. Time-resolved UV−visible spectra were recorded with a Hewlett-Packard Model 8453 diode array rapid-scanning spectrophotometer.

Microanalyses were performed at the Université de Bourgogne on a Fisons EA 1108 CHNS instrument. Mass spectra were obtained either with a Bruker Ultraflex II instrument in MALDI-TOF reflectron mode using dithranol (1,8-dihydroxy-9[10H]-anthracene) as a matrix, or on a Bruker MicroToFQ instrument in ESI mode.

Chemicals and Reagents. Pyridine (py, 99.8%) and tetra-*n*-butylammonium chloride (TBACl, ≥ 99%) were obtained from Sigma-Aldrich Chemical Co. and used without further purification. Benzonitrile (PhCN) was purchased from Aldrich Chemical Co. and distilled over P_2O_5 under vacuum prior to use. Absolute dichloromethane (CH_2Cl_2, 99.8%) was received from EMD Chemicals Inc. and used without further purification. Tetra-*n*-butylammonium perchlorate (TBAP, ≥ 99%) and tetrabutylammonium acetate (TBAOAc, ≥ 99%) were purchased from Fluka Chemical Co. and used as received. Neutral alumina (Merck; usually Brockmann grade III, i.e., deactivated with 6% water) or Silica gel (Merck: 70−120 μm) was used for column chromatography. Analytical thin layer chromatography was performed using Merck 60 F254 neutral Aluminum oxide gel (precoated sheets, 0.2 mm thick) or Merck 60 F254 silica gel (precoated sheets, 0.2 mm thick). Reactions were monitored by thin layer chromatography and spectrophotometry.

The Mn(III) monocorrole (Mes_2PhCor)Mn (**1**),[25] and the free-base porphyrin-corrole dyads[39−41] ($PMes_2CX$)H_5 and ($PMes_2CA$)H_5, were prepared as reported in the literature. Other syntheses were carried out as described below.

(2,8,12,18-Tetraethyl-3,7,13,17-tetramethyl-5-phenylporphyrin)-chloromanganese (Et_4Me_4PhP)MnCl (2). A solution of 225 mg (0.46 mmol) of (Et_4Me_4PhP)H_2 and 450 mg of $Mn(OAc)_2\cdot 4H_2O$ in 50 mL of DCE/MeOH: 75/25 was heated under nitrogen at 85 °C for 2 h. The solvent was removed in vacuum, and the residue was passed through a column of silica using methylene chloride first and then methylene chloride/methanol (90/10) as eluents. The fraction containing the desired compound was washed by a 1 M water solution of HCl, then with water, and dried over magnesium sulfate. After evaporation, the chloro derivative was obtained as a blackish-brown powder in 92% yield (257 mg). MS (MALDI-TOF): m/z = 607.042 $[M - Cl]^+$, 607.263 Calcd. for $C_{38}H_{40}MnN_4$. HR-MS (ESI): m/z = 607.2724 $[M - Cl]^+$, 607.2633 Calcd. for $C_{38}H_{40}MnN_4$.

4-[Manganese-(5,15-dimesitylcorrol-10-yl)]-5-[acetatomanganese-(13,17-diethyl-2,3,7,8,12,18-hexamethylporphyrin-5-yl)]-9,9-dimethylxanthene ($PMes_2CX$)Mn_2(OAc) (3OAc). Under nitrogen and shielded from light, a mixture of 65 mg of ($PMes_2CX$)H_5 (0.054 mmol, 1 equiv) and 54 mg of $Mn(OAc)_2\cdot 4H_2O$ (0.22 mmol, 4 equiv) in 70 mL of 1,2-dichloroethane/ethanol (4/1) was heated at 85 °C for 16 h. The reaction mixture was then allowed to cool to room temperature and washed with water (3×75 mL), dried over $MgSO_4$, and then evaporated. The remaining residue was chromatographed on silica (CH_2Cl_2/methanol 90/10 as eluent), and the last fraction was collected to give the title biscorrole bismanganese complex (**3OAc**) in 89% yield (63 mg, 0.048 mmol). MS (MALDI-TOF): m/z = 1295.44 $[M - CH_3COO]^+$. HR-MS (ESI): m/z = 1354.4796 $[M]^{+\bullet}$, 1354.4801 Calcd. for $C_{84}H_{76}Mn_2N_8O_3$.

1-[Manganese-(5,15-dimesitylcorrol-10-yl)]-8-[acetatomanganese-(13,17-diethyl-2,3,7,8,12,18-hexamethylporphyrin-5-yl)]-anthracene ($PMes_2CA$)Mn_2(OAc) (4OAc). This compound was prepared in 88% yield (80 mg, 0.063 mmol), as described for ($PMes_2CX$)Mn_2, starting from ($PMes_2CA$)H_5 (83 mg, 0.065 mmol, 1 equiv) and $Mn(OAc)_2$ (65 mg, 0.26 mmol, 4 equiv). MS (MALDI-TOF): m/z = 1263.41 $[M\text{-}CH_3COO]^+$. HR-MS (ESI): m/z = 1322.4500 $[M]^{+\bullet}$, 1322.4539 Calcd. for $C_{83}H_{72}Mn_2N_8O_2$.

4-[Manganese-(5,15-dimesithylcorrol-10-yl)]-6-[acetatomanganese-(13,17-diethyl-2,3,7,8,12,18-hexamethylporphyrin-5-yl)]-dibenzofuran ($PMes_2CO$)Mn_2(OAc) (5OAc). Under nitrogen and shielded from light, a mixture of 145 mg of ($PMes_2CO$)H_5 (0.126 mmol, 1 equiv) and 123 mg of $Mn(OAc)_2$ (0.50 mmol, 4 equiv) in 50 mL of 1,2-dichloroethane/methanol/ethanol (7/2/3) was refluxed for 24 h. The reaction mixture was then allowed to cool to room temperature and washed with water (3 × 75 mL), dried over $MgSO_4$, and then evaporated. The remaining residue was chromatographed on silica (CH_2Cl_2/methanol 50/50 as eluent) and the last fraction was collected to give the title porphyrin-corrole bismanganese complex in 70% yield (110 mg, 0.088 mmol). MS (MALDI-TOF): m/z = 1253.37 $[M - CH_3COO]^+$. HR-MS (ESI): m/z = 1312.4306 $[M]^{+\bullet}$, 1312.4326 Calcd. for $C_{81}H_{70}Mn_2N_8O_3$.

2-[(Manganese-5,15-dimesitylcorrol-10-yl)-2′-(acetatomanganese-13,17-diethyl-2,3,7,8,12,18-hexamethylporphyrin-5-yl)]-diphenylether ($PMes_2COx$)Mn_2(OAc) (6OAc). This compound was prepared in 75% yield (42 mg, 0.031 mmol), as described for ($PMes_2CO$)Mn_2(OAc), starting from ($PMes_2COx$)H_5 (50 mg, 0.040 mmol, 1 equiv) and $Mn(OAc)_2$ (40 mg, 0.16 mmol, 4 equiv). MS (MALDI-TOF): m/z = 1255.43 $[M - CH_3COO]^+$. HR-MS (ESI): m/z = 1314.4419 $[M]^{+\bullet}$, 1314.4483 Calcd. for $C_{81}H_{72}Mn_2N_8O_3$.

Dyads **3**−**6** were quantitatively obtained by washing the corresponding dichloromethane solution of the above acetate containing derivatives with a 1 M hydrochloric acid solution. MALDI-TOF analysis of the compounds gave $[M - Cl]^+$ as the unique ion of the spectrum.

Dyad 3. UV−vis (CH_2Cl_2), λ_{max} (nm) ($\varepsilon \times 10^{-3}$, mol^{-1} L cm^{-1}): 364 (67), 402 (45), 420 (40), 472 (31), 561 (11), 646 (6), 772 (2).

dx.doi.org/10.1021/ic102399g |*Inorg. Chem.* 2011, 50, 3479–3489

Dyad 4. UV−vis (CH_2Cl_2), λ_{max} (nm) ($\varepsilon \times 10^{-3}$, mol^{-1} L cm^{-1}): 364 (75), 397 (44), 427 (38), 468 (47), 558 (15), 641 (8), 783 (3).
Dyad 5. UV−vis (CH_2Cl_2), λ_{max} (nm) ($\varepsilon \times 10^{-3}$, mol^{-1} L cm^{-1}): 363 (80), 399 (44), 429 (39), 472 (47), 562 (13), 645 (7), 781 (1.5).
Dyad 6. UV−vis (CH_2Cl_2), λ_{max} (nm) ($\varepsilon \times 10^{-3}$, mol^{-1} L cm^{-1}): 363 (83), 400 (49), 420 (42), 475 (51), 563 (14), 645 (6), 774 (0.2).

RESULTS AND DISCUSSION

Structures of the investigated bis-manganese and monomanganese derivatives are given in Chart 1. Each manganese complex was prepared in good yield starting from the corresponding free-base porphyrin-corrole dyad.[39−41] Because $Mn(OAc)_2$ was used as metalating agent, the bismanganese porphyrin-corrole derivatives initially contained acetate ion bound to the Mn(III) porphyrin part of the dyad (see later structure) but OAc^- was then replaced by Cl^- after reacting the derivatives with 1 M hydrochloric acid solution, leading to the actually investigated dyads **3**−**6**.

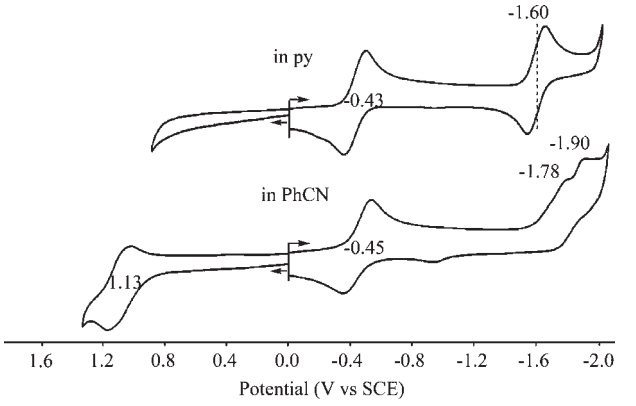

Figure 1. Cyclic voltammograms of $(Et_4Me_4PhP)MnCl$ **2** in pyridine and PhCN containing 0.1 M TBAP, scan rate = 0.1 V/s.

UV−visible Spectroscopy. UV−visible absorption maxima and molar absorptivities of dyads **3**−**6** and the structurally related monomers **1** and **2** are summarized in the Experimental Section, and a compilation of UV−visible data under different solvent conditions is given in Supporting Information, Table S1. The monomeric manganese(III) porphyrin **2** has a split Soret band (at 361 and 472 nm) in addition to two weak visible bands at 568−593 nm and one weaker near-IR band at 776 nm. This morphology resembles that of others manganese(III) monoporphyrins and is due to a d-type hyperporphyrin character resulting from significant metal-porphyrin π interactions in these Mn^{III} complexes.[42]

Because molar absorptivities of bands associated with the corrole part of the dyads **3**−**6** are much weaker than those associated with the porphyrin part of the molecule, spectral patterns of these compounds are dominated by the porphyrin absorptions, and the overall UV−visible spectra are quite similar to that of the monoporphyrin analogue **2**. However, the spectrum of the dyads **3**−**6** can actually be treated as a simple sum of absorptions associated with the individual Mn(III) porphyrin and Mn(III) corrole macrocyclic units. For example, the split Soret band (363−364 and 468−475 nm) and single weak near IR bands (772−783 nm) in

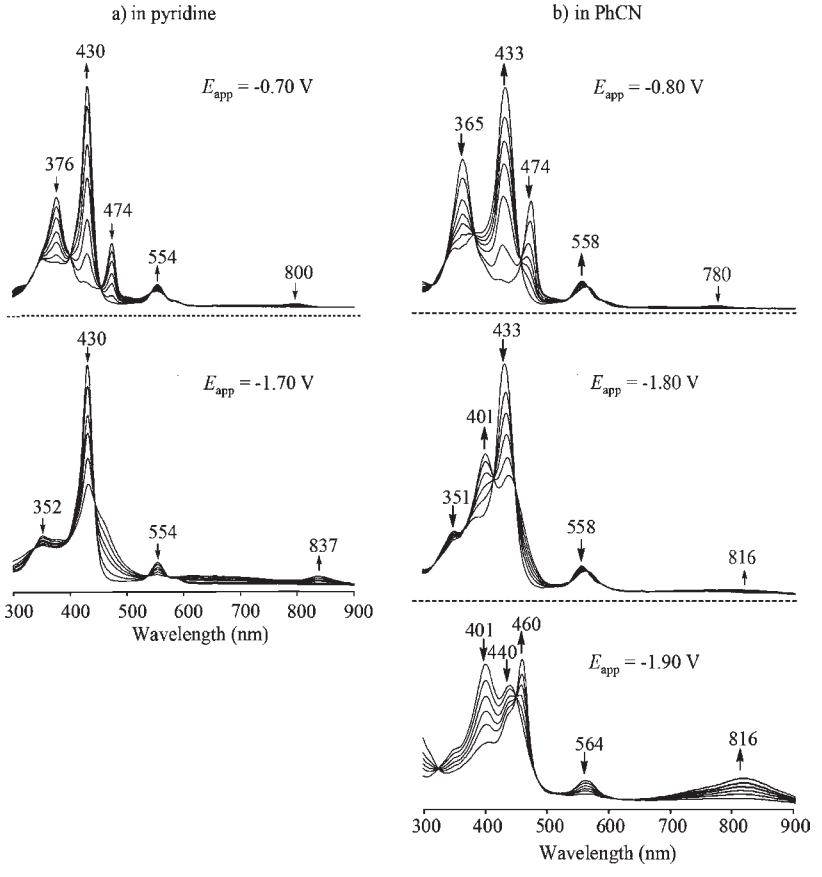

Figure 2. UV−visible spectral changes of $(Et_4Me_4PhP)MnCl$ (**2**) in (a) pyridine and (b) PhCN containing 0.1 M TBAP under application of the indicated applied potentials.

dx.doi.org/10.1021/ic102399g |*Inorg. Chem.* 2011, 50, 3479–3489

the UV−vis spectra of **3**−**6** in CH_2Cl_2 are clearly attributed to the porphyrin macrocycle while the two shoulder bands appearing at about 397−400 nm and 420−427 nm in the spectra of these compounds are assigned as contributions from the corrole macrocycle. Furthermore, the overlapping Q-bands associated with the two different macrocycles in the dyads **3**−**6** gives what appears to be a single broad visible band from 558 to 645 nm in the spectrum. As shown later in the manuscript, this information proves to be quite useful in independently assigning the site of each electron transfer on the basis of the spectroelectrochemical data.

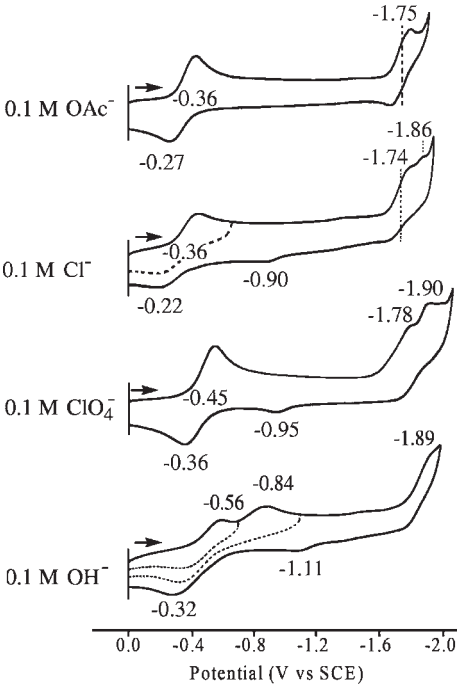

Figure 3. Cyclic voltammograms of $(Et_4Me_4PhP)MnCl$ **2** in PhCN containing 0.1 M TBAX (X = Cl^-, OAc^-, ClO_4^-, and OH^-). Scan rate = 0.1 V/s.

Mass Spectrometry. A $(PMes_2C)Mn_2$ fragment is systematically detected for **3**−**6** but not the molecular peak in the MALDI mode. Therefore the main ionic pattern corresponds to a dyad having lost the Cl^- axial ligand initially bound to the Mn(III) center of the porphyrin macrocycle. Conversely, the molecular ion could be observed for compounds **3**−**6(OAc)** in ESI ionization mode with excellent agreement between the calculated and experimental measurements (See Experimental Section). In all cases, the mass spectral data agree well with the proposed structural arrangement, that is, the bimetallic nature of each compound.

ESR Characterization. ESR experiments were carried out at room temperature and also at liquid nitrogen temperature at X-band frequencies. In no cases were ESR signals observed for the bis-manganese complexes, either at room temperature in toluene solutions or in frozen toluene at 77 K. Indeed, such complexes often display a zero-field splitting energy term (D) on the order of 1−4 cm^{-1} and thus the allowed $\Delta m_s = \pm 1$ transitions of the manganese(III) porphyrins and corroles are not detectable at X-band frequencies by perpendicular polarization of the microwave field.[43−45]

Electrochemistry and Spectroelectrochemistry of Mn(III) Monoporphyrin 2. To better understand electrochemical behavior of the investigated porphyrin-corrole dyads **3**−**6**, it was necessary to first elucidate redox and ligand binding properties of the related monoporphyrin **2** under the same solution conditions as the dyads. This is described on the following pages, first for the monoporphyrin **2** and then for the porphyrin-corrole dyads **3**−**6**. Electrochemical properties of the monocorrole **1** have been described in the literature under several solution conditions.[25]

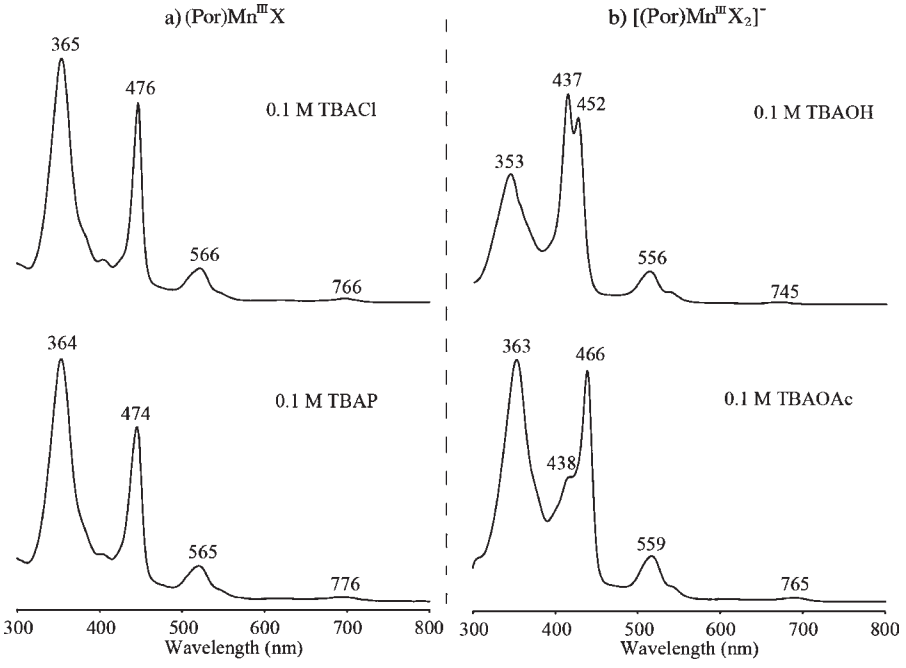

Figure 4. UV−visible spectra of $(Et_4Me_4PhPor)MnCl$ **2** in PhCN containing 0.1 M TBAX to give (a) $(Por)Mn^{III}X$ where X = Cl^- or ClO_4^- and (b) $[(Por)Mn^{III}X_2]^-$ where X = OH^- or OAc^- and Por represents Et_4Me_4PhPor.

dx.doi.org/10.1021/ic102399g |*Inorg. Chem.* 2011, 50, 3479–3489

Scheme 1. Redox Reaction of Monoporphyrin 2 under Different Solution Conditions

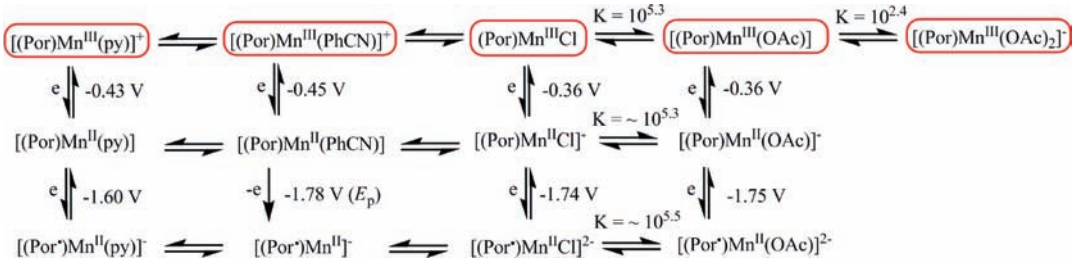

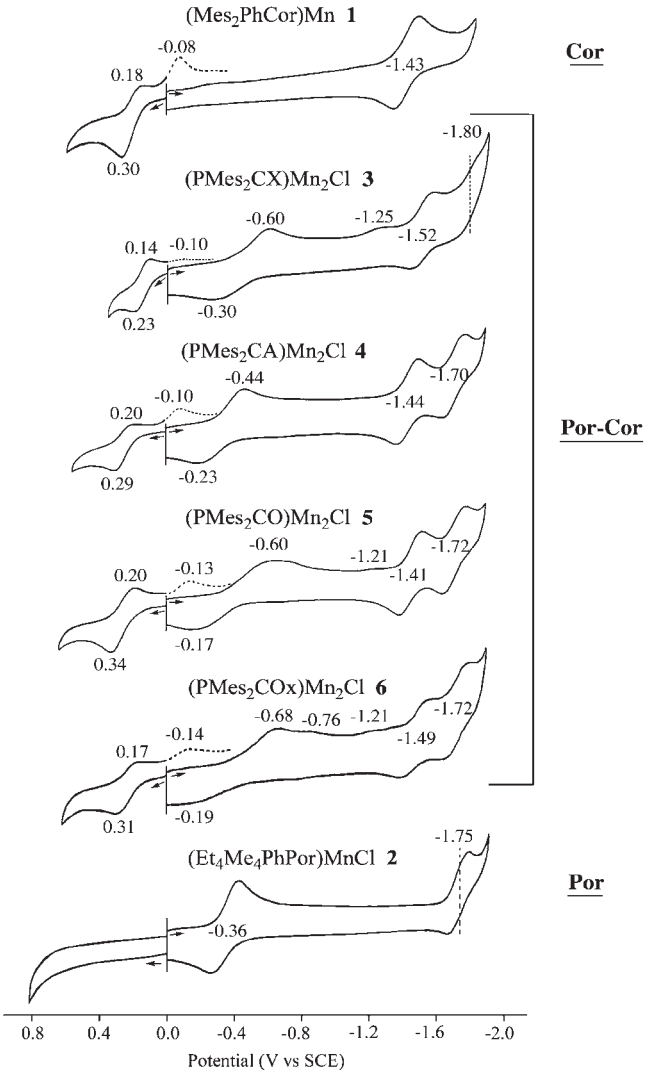

Figure 5. Comparison of cyclic voltammograms for monocorrole **1**, monoporphyrin **2**, and porphyrin-corrole dyads **3**−**6** in PhCN containing 0.1 M TBAOAc at scan rate of 0.1 V/s.

Cyclic voltammograms of **2** in pyridine and PhCN containing 0.1 M TBAP are displayed in Figure 1. Two reversible reductions are observed in pyridine at $E_{1/2}$ = −0.43 and −1.60 V while in PhCN the first reduction at $E_{1/2}$ = −0.45 V is followed at more negative potentials by two irreversible processes at E_p= −1.78 and −1.90 V for a scan rate of 0.1 V/s. The monoporphyrin **2** also exhibits a reversible one-electron oxidation at $E_{1/2}$ = 1.13 V

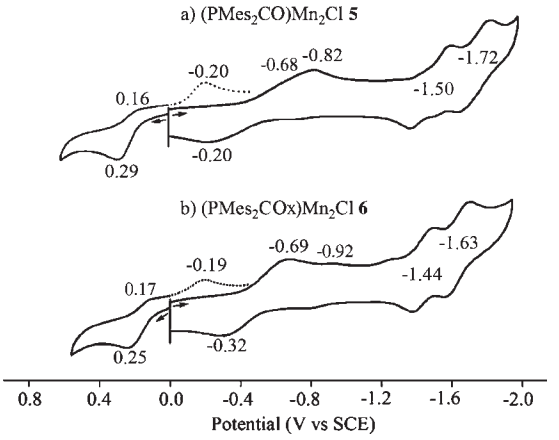

Figure 6. Cyclic voltammograms of (a) **5** and (b) **6** in pyridine containing 0.1 M TBAOAc at scan rate of 0.1 V/s.

in PhCN, but this process could not be monitored in pyridine because of the limited anodic potential window of solvent. Similar electrochemical behavior was previously reported for the structurally related $(Et_2Me_6PhP)MnCl$, in PhCN[46] and pyridine.[24]

The first reduction of **2** involves a Mn^{III}/Mn^{II} process in both solvents, and this was confirmed by thin-layer spectroelectrochemistry where almost identical spectral changes are seen in pyridine (Figure 2a) and PhCN (Figure 2b). The diagnostic absorption band assigned to the Mn(II) form of the porphyrin is located at 430 nm in pyridine and 433 nm in PhCN, and this can be compared to a 430 nm band for $(Et_2Me_6PhP)Mn^{II}$ in pyridine, as earlier reported in the literature.[12]

Although similar spectral changes are seen for the Mn(III)/Mn(II) process of **2** in pyridine and PhCN, significant differences exist between spectra of the doubly reduced products in these two solvents. For example, controlled potential reduction of **2** at −1.80 V in pyridine results in a loss of the Soret band intensity and the appearance of an 837 nm band which is characteristic of a porphyrin π-anion radical (Figure 2a), while the UV−vis spectrum of doubly reduced **2** in PhCN exhibits a new band at 401 nm, and it also has a broad near-IR band at ~816 nm (Figure 2b).

Shifting the applied potential from −1.80 to −1.90 V in PhCN leads to further changes in the UV−vis spectra including an increased intensity of the 816 nm band (see Figure 2b), but because the last two electrode reactions of **2** are irreversible and close to the negative potential limit of the PhCN solvent, these processes were not examined in further detail.

dx.doi.org/10.1021/ic102399g |*Inorg. Chem.* 2011, 50, 3479–3489

Table 1. Half-Wave and Peak Potentials (V vs SCE) of Bis-Manganese Porphyrin-Corrole Dyads in PhCN or Pyridine, 0.1 M TBAOAc

			oxidation	reduction			
solvent	compound		(Cor)Mn^{III}/Mn^{IV}	(Por)Mn^{III}/Mn^{II}		(Cor)Mn^{III}/Mn^{II}	Por ring
PhCN	$(Mes_2PhCor)Mn$	**1**	0.24 (-0.08^{Epc})			−1.43	
	$(Et_4Me_4PhP)MnCl$	**2**		−0.36			−1.75
	$(PMes_2CX)Mn_2Cl$	**3**	0.19 (-0.10^{Epc})	−0.60[a]		−1.52	−1.80
	$(PMes_2CA)Mn_2Cl$	**4**	0.25 (-0.10^{Epc})	−0.44[a]		−1.44	−1.70
	$(PMes_2CO)Mn_2Cl$	**5**	0.27 (-0.13^{Epc})	−0.60[a]	−0.74[a]	−1.41	−1.72
	$(PMes_2COx)Mn_2Cl$	**6**	0.24 (-0.14^{Epc})	−0.68[a]	−0.76[a]	−1.49	−1.72
pyridine	$(Mes_2PhCor)Mn$	**1**	0.21 (-0.09^{Epc})			−1.40	
	$(Et_4Me_4PhP)MnCl$	**2**		−0.38			−1.59
	$(PMes_2CO)Mn_2Cl$	**5**	0.23 (-0.20^{Epc})	−0.68[a]	−0.82[a]	−1.50	−1.72
	$(PMes_2COx)Mn_2Cl$	**6**	0.21 (-0.19^{Epc})	−0.69[a]	−0.92[a]	−1.44	−1.63

[a] Peak potential at a scan rate of 0.1 V/s; E_{pc} = additional reoxidation peak seen on reverse scan

The monoporphyrin $(Et_4Me_4PhP)MnCl$ **2** was also electrochemically studied in PhCN containing 0.1 M TBAX where X = OAc^-, Cl^-, or OH^- to better understand how the binding of these anions would effect redox potentials and spectroscopic properties of the porphyrin-corrole dyads under the same solution conditions.

As seen in Figure 3, the potentials and reversibility for the electroreductions of **2** in PhCN depend markedly upon the anions in solution, and this can be accounted for by differences in axial coordination at the Mn(III) and Mn(II) centers of the porphyrin. The most reversible processes occur in PhCN solutions with 0.1 M TBAOAc as supporting electrolyte ($E_{1/2}$ = −0.36 and −1.75 V), and this is followed by PhCN containing 0.1 M TBACl where the first two reductions are reversible to quasi-reversible and located at $E_{1/2}$ = −0.36 and −1.74 V.

As discussed in later sections of the manuscript, OAc^- strongly binds to the manganese porphyrin both before and after electroreduction, forming five- and six-coordinate complexes in the case of the Mn(III) monoporphyrin but only a five-coordinate species in the case of the Mn(II) derivative. This result is consistent with the known coordination chemistry of synthetic manganese porphyrins.[47−49] As seen in Figure 3, the first reduction of **2** in 0.1 M $TBAClO_4$ is reversible and located at $E_{1/2}$ = −0.45 V while in 0.1 M TBAOH, the Mn(III)/Mn(II) process is split into two peaks at E_p = −0.56 and −0.84 V for a scan rate 0.1 V/s. The split processes in the hydroxide solution is consistent with two different forms of axially coordinated Mn(III) being involved in the electron transfer under the given solution conditions.

In the PhCN solution containing 0.1 M TBACl or 0.1 M TBAOAc, the reversible process at $E_{1/2}$ = −0.36 V is proposed to involve reduction of a five-coordinate (Por)$Mn^{III}X$ to its anionic five-coordinate $[(Por)Mn^{II}X]^-$ form (eq 1) while in 0.1 M TBAOH, the electrode reactions most likely involve a reduction of $[(Por)Mn^{III}(OH)_2]^-$ (E_p = −0.84 V) and (Por)Mn^{III}(OH) (E_p = −0.56 V) to give the same $[(Por)Mn^{II}(OH)]^-$ product as shown in eqs 2 and 3.

$$(Por)Mn^{III}X + e \rightleftharpoons [(Por)Mn^{II}X]^- \qquad E_{1/2} = -0.36\ V \qquad (1)$$

$$(Por)Mn^{III}(OH) + e \rightleftharpoons [(Por)Mn^{II}(OH)]^- \qquad E_p = -0.56\ V \qquad (2)$$

$$[(Por)Mn^{III}(OH)_2]^- + e \rightleftharpoons [(Por)Mn^{II}(OH)]^- + OH^- \qquad E_p = -0.84\ V \qquad (3)$$

An anionic six-coordinate $[(Por)Mn^{III}(OAc)_2]^-$ complex can also be generated in PhCN solutions upon addition of TBAOAc as shown by the UV−vis spectra of **2** in PhCN containing 0.1 M TBAX where X = Cl^-, ClO_4^-, OH^-, and OAc^- (Figure 4a). The two spectra assigned to (Por)$Mn^{III}X$ are virtually identical for X = Cl^- and ClO_4^- while similar spectral patterns are obtained for $[(Por)Mn^{III}X_2]^-$ where X = OH^- and OAc^- (Figure 4b). The main difference between the latter two spectra is that the bis-OH^- complex of **2** is fully formed in PhCN solutions containing 0.1 M TBAOH but a mixture of mono and bis-acetate Mn(III) derivatives are obtained in PhCN containing 0.1 M TBAOAc (Supporting Information, Figure S1).

Despite the fact that two forms of acetate-bound Mn(II) are present in the PhCN solution, the reversibility of the Mn(III)/Mn(II) process is easily explained by a conversion of $[(Por)Mn^{III}(OAc)_2]^-$ to the more easily reducible $[(Por)Mn^{III}(OAc)]$ under the application of a potential prior to generation of the Mn(II) porphyrin, thus leading to a reversible electrode reaction at $E_{1/2}$ = −0.36 V (Figure 3). These electrode reactions of the monoporphyrin **2** in solution of TBAOAc are summarized in Scheme 1 which also includes data in PhCN and pyridine containing 0.1 M TBAP or TBACl as supporting electrolytes.

Porphyrin-Corroles. Each porphyrin-corrole dyad (**3**−**6**) was investigated in PhCN and pyridine containing 0.1 M TBAOAc or 0.1 M $TBAClO_4$. Examples of the resulting cyclic voltammograms for all four dyads in the PhCN solvent with the two different supporting electrolytes are shown in Figures 5 (TBAOAc) and Supporting Information, Figure S2 ($TBAClO_4$) which also include data for the monocorrole **1** and monoporphyrin **2** while cyclic voltammograms in pyridine containing 0.1 M TBAOAc are shown in Figure 6 for compounds **5** and **6**.

As seen from these figures, electrochemical behavior of the porphyrin-corrole dyads varies with the solvent (pyridine or PhCN), type of anion added to solution as supporting electrolyte (ClO_4^- or OAc^-), and type of bridge separating the two macrocycles in a face-to-face arrangement. Pyridine and OAc^- both strongly bind to the monoporphyrin **2** in its Mn(III) and Mn(II) oxidation states (see Scheme 1), while pyridine and acetate ion

dx.doi.org/10.1021/ic102399g |*Inorg. Chem.* 2011, 50, 3479–3489

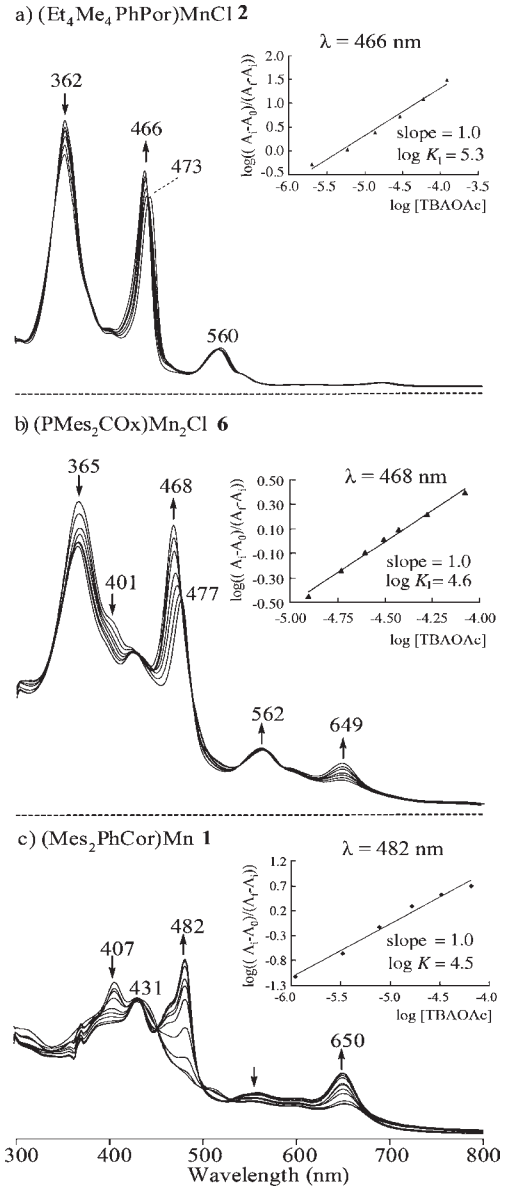

Figure 7. UV−visible spectral changes of (a) (Et_4Me_4PhPor)MnCl **2**, (b) ($PMes_2COx)Mn_2Cl$ **6**, and (c) (Mes_2PhCor)Mn **1** in PhCN during addition of TBAOAc (inset shows the Hill plot).

Table 2. Binding Constants (log *K*) of the Monocorrole 1, the Monoporphyrin 2, and Dyads 3−6 with OAc^- in PhCN

compound		log K_1	log K_2
(Mes_2PhCor)Mn	**1**	4.5	
(Et_4Me_4PhP)MnCl	**2**	5.3	2.4
($PMes_2CX)Mn_2Cl$	**3**	5.0	2.0
($PMes_2CA)Mn_2Cl$	**4**	4.9	2.5
($PMes_2CO)Mn_2Cl$	**5**	5.2	2.3
($PMes_2COx)Mn_2Cl$	**6**	4.6	*a*

[a] The second ligand addition was not observable by UV−vis spectral methods in solutions containing up to 0.1 M TBAOAc.

bind to the monocorrole **1** in its Mn(IV), Mn(III), and Mn(II) oxidation states as previously described in the literature.[25]

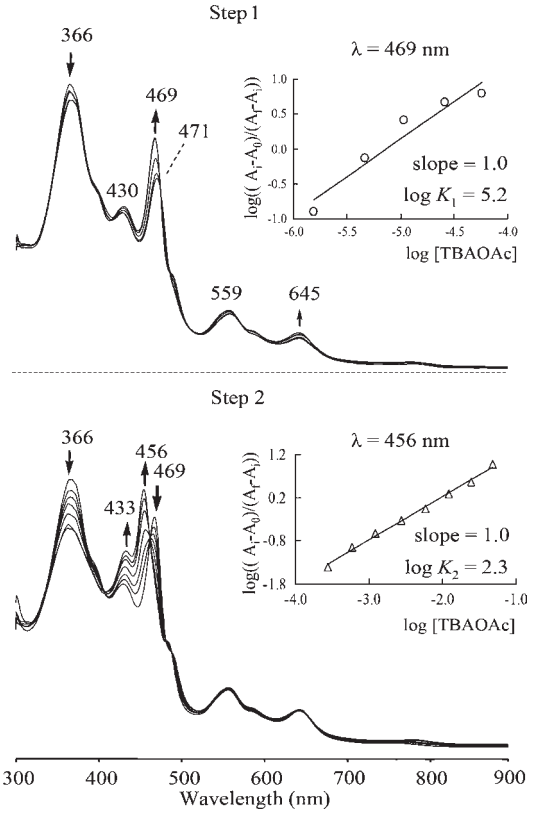

Figure 8. Two-step spectral changes of ($PMes_2CO)Mn_2Cl$ **5** ($\sim 10^{-5}$ M) in PhCN during addition of TBAOAc (inset shows the Hill plot).

Scheme 2. Acetate Binding Reaction of Dyads 3−6 in PhCN

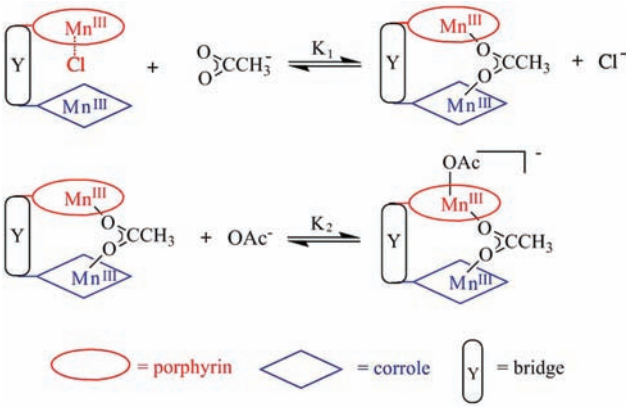

The following observation can be made regarding the cyclic voltammograms in Figures 5 and 6. The electrochemical behavior of the dyads in PhCN containing 0.1 M TBAOAc closely resembles that of the individual macrocyclic units for the two electrode reactions of the corrole and also for the second, but not the first, reduction of the porphyrin. For example, conversion of the Mn(III) monocorrole **1** to its Mn(IV) form in PhCN, 0.1 M TBAOAc is characterized by a single one electron oxidation at E_p = 0.30 V, and this is followed by two coupled re-reduction peaks, the first at E_{pc} = 0.18 V and the second at E_p = −0.08 V for a scan rate of 0.1 V/s. The same voltammetric pattern is seen for the

dx.doi.org/10.1021/ic102399g |*Inorg. Chem.* 2011, 50, 3479–3489

dyads **3**−**6** in PhCN as well as in pyridine containing 0.1 M TBAOAc. The reversible one electron reduction of the monocorrole **1** occurs at −1.43 V, and the reversible one electron reduction of the corrole unit in the dyads **3**−**6** is located at $E_{1/2}$ = −1.41 to −1.52 V, again both in PhCN (Figure 5) and in pyridine (Figure 6). At the same time, the ring-centered reduction of the Mn(II) porphyrin appears at $E_{1/2}$ = −1.75 V in PhCN, 0.1 M TBAOAc, and a similar reversible reduction is seen for the dyads **4**−**6** at $E_{1/2}$ = −1.63 to −1.72 V, the exact value depending upon the solvent and the spacer (see summary of potentials in Table 1).

The difference in electrochemical behavior between the corrole or porphyrin macrocycle found in the dyads and the same electrode reactions of the monomacrocycles is related not only to the specific spacer which determines the distance between the two conjugated π-systems but also to the fact that one acetate ligand binds within the cavity and is coordinated to both the porphyrin and the corrole units as shown by the X-ray structure for **5OAc** in Supporting Information, Figure S3.

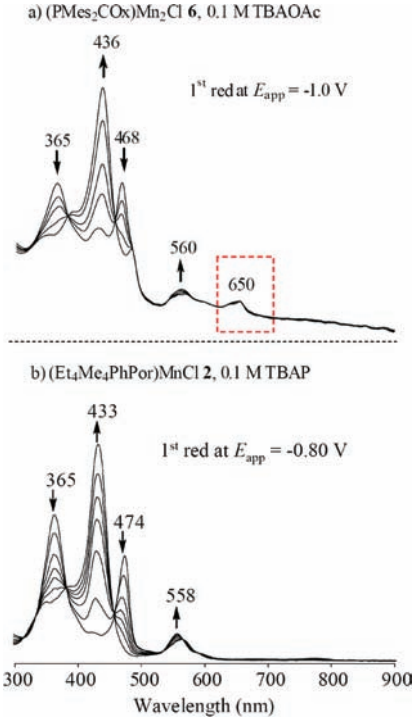

Figure 9. UV−visible spectral changes during the first reduction in PhCN of (a) $(PMes_2COx)Mn_2Cl$ **6** with 0.1 M TBAOAc and (b) $(Et_4Me_4PhPor)MnCl$ **2** with 0.1 M TBAP. Mn(II) porphyrin and no change in intensity of the 650 nm band which is diagnostic of a Mn(III).

Binding of a single OAc^- ligand to both the corrole and the porphyrin is also suggested by UV−visible spectral measurements taken during titration of the monomacrocycles and **3**−**6** with TBAOAc in PhCN. An example is given in Figure 7b for the case of **6** where log K = 4.6 as calculated by the diagnostic log−log plot shown in the inset of the figure. The acetate-bound dyad product has bands at 365, 468, and 562 nm as compared to 362, 466, and 560 nm for the product formed after addition of one OAc^- ligand to the monoporphyrin **2** under the same solution conditions (Figure 7a). There is also a band for the ligated dyad at 649 nm which compares to a 650 nm band for the monocorrole **1** with one added OAc^- ligand (see Figure 7c and ref 25). The three sets of spectra in Figure 7 are thus self-consistent and provide additional evidence for formulation of $(PMes_2COx)Mn_2(OAc)$ in solutions of PhCN containing added TBAOAc.

Manganese(III) porphyrins are known to bind two axial ligands as described earlier in the manuscript for the monoporphyrin **2**, and two acetate ligands will also bind to the porphyrin part of the dyads **3**−**6** in PhCN containing high concentrations of TBAOAc. One of the coordinated acetates is located inside the cavity and also bound to the Mn(III) center of the corrole while a second OAc^- ligand can coordinate on the opposite side of the porphyrin plane to give the six-coordinate Mn(III) porphyrin complex.

Calculated binding constants for the stepwise addition of two OAc^- axial ligands to **3**−**6** are summarized in Table 2, and an example of the spectral changes which occur during these processes is shown in Figure 8 for compound **5** where the products of the first and second acetate additions have major absorption bands at 469 and 456 nm, respectively. The two acetate additions to **3**−**6** proceed in a similar manner as shown Scheme 2. The coordination of OAc^- to both manganese ions within the cavity affects not only the values of half wave potentials but also the reversibility of the electron transfer reactions. This latter effect is most evident in the case of the Mn^{III}/Mn^{II} porphyrin reaction which is reversible for **2** in PhCN solutions containing 0.1 M TBAOAc, TBAP, or TBACl

Scheme 3. Proposed Overall Mechanism for Oxidation and Reduction of Dyads in PhCN[a]

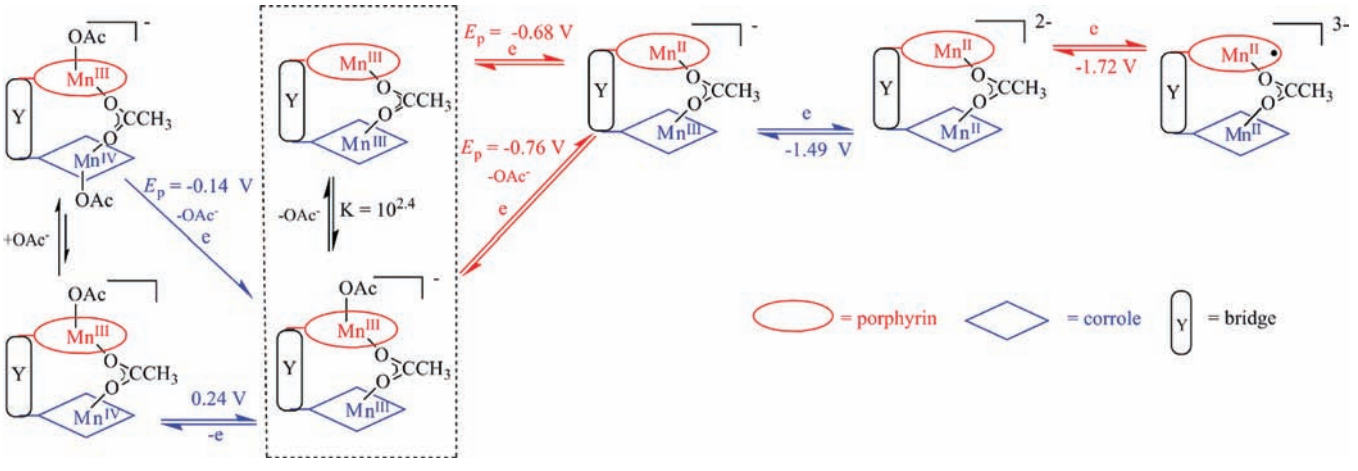

[a] Listed potentials are for Compound **6** at scan rate of 0.1 V/s.

dx.doi.org/10.1021/ic102399g |Inorg. Chem. 2011, 50, 3479–3489

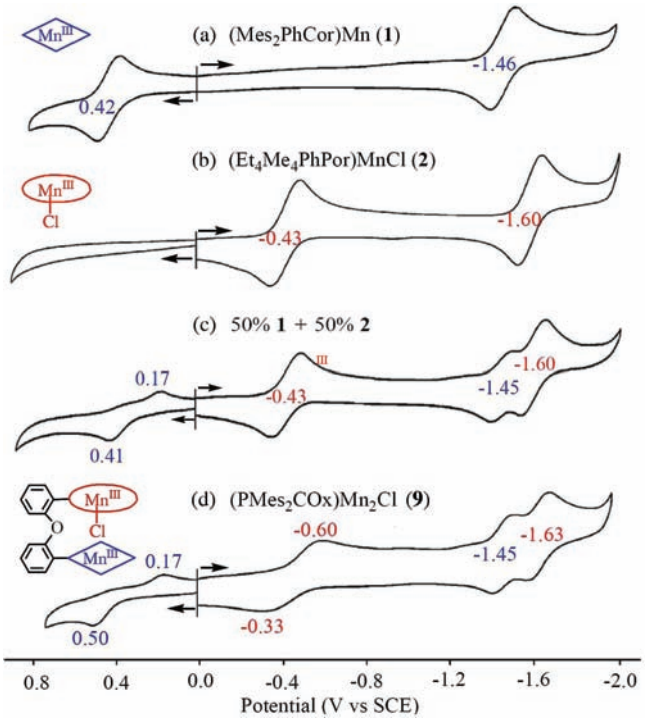

Figure 10. Cyclic voltammograms of monomeric macrocycles (Mes_2PhCor)Mn **1** and (Et_4Me_4PhPor)MnCl **2**, and the dyad ($PMes_2COx$)Mn_2Cl **6** in pyridine; (a), (b), (c), and (d) in pyridine containing 0.1 M TBAP at scan rate of 0.1 V/s.

(Figure 3) but quasi-reversible for **3**−**6** in PhCN or pyridine containing 0.1 M TBAOAc (Figures 5 and 6).

It has long been known that metal-centered reductions of synthetic Mn(III) porphyrins significantly depend upon the number of axial ligands coordinated to the Mn(III) and Mn(II) forms of the compounds.[48,50] Reversible to quasi-reversible reductions are obtained under conditions where there is no change in the number of bound axial ligands during electron transfer while slow (irreversible to quasi-reversible) electron transfer reactions are obtained when a six-coordinate Mn(III) porphyrin is reduced to its five-coordinate form. This change in rate of electron transfer is related to changes in the Mn(III) and Mn(II) out of plane distance upon going from the six-coordinate reactant to the five-coordinate product as earlier described in studies by Mu and Schultz.[48]

Acetate Binding to Electroreduced Dyads. The single acetate ion located within the cavity of the dyads and bound to the Mn(II) centers of both macrocycles remains coordinated after addition of at least two and possible three electrons to the neutral dyads when the reaction is carried out in PhCN containing 0.1 M TBAOAc. Evidence in support of this assignment after the first porphyrin reduction is given for **6** in part by the known coordination chemistry of Mn(II) porphyrins and Mn(II) corroles and in part by the thin-layer spectroelectrochemical data in Figure 9 which shows an intense Soret band at 436 nm for the product indicating formation of a corrole containing the bound acetate ligand.

The shape of the cyclic voltammograms in Figure 5 also provides evidence for coordination of OAc^- to the Mn(II) porphyrin and Mn(II) corrole in the dyad, namely, the reversible corrole oxidation at −1.44 to −1.49 V is seen only after

Scheme 4. Proposed Mechanism of the First Oxidation of the Porphyrin-Corrole Dyads in Pyridine

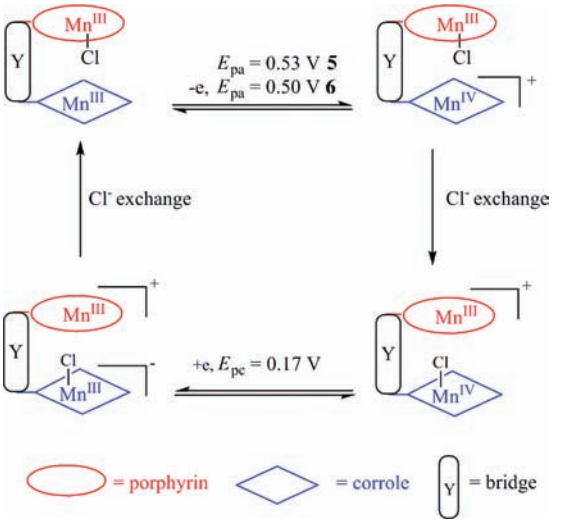

coordination of an anionic axial ligand, and the same can be said for the reversible porphyrin reaction at −1.72 to −1.75 V (see examples in Figure 5, Supporting Information, Figure S2, and ref 25). These reactions are summarized in Scheme 3.

Chloride Ion Exchange during Electrooxidation. As earlier indicated, each redox process of the porphyrin-corrole dyads can, in most cases, be assigned by comparing the potentials and reversibility of individual electron transfer reactions with that of the monocorrole **1** and the monoporphyrin **2** under the same solution conditions. One example is given in Figure 10 for the dyad **6** in pyridine. As shown in this figure, the cyclic voltammogram of this dyad in pyridine containing 0.1 M TBAP (Figure 10d) is quite similar to that of a 1:1 mixture of **1** and **2** under the same solution conditions (Figure 10c). The main difference between the two current−voltage curves in Figures 10c and 10d is the process assigned to the Mn^{III}/Mn^{II} reaction of the porphyrin which is reversible in the mixture or in solutions not containing the corrole ($E_{1/2}$ = −0.43 V) but becomes quasi-reversible to irreversible in the case of the dyad where E_{pc} = −0.60 and E_{pa} = −0.33 V for a scan rate of 0.1 V/s.

The chemical reaction following the corrole-centered oxidation of **6** at E_{pa} = 0.50 V in Figure 10d involves a rapid binding of Cl^- to the electrogenerated Mn(IV) corrole as determined by analysis of data in the literature[25] and additional experiments carried out in the present study. While the oxidation of the monocorrole **1** is reversible in pyridine containing 0.1 M TBAP (Figure 10a, $E_{1/2}$ = 0.42 V), it becomes irreversible in the 1:1 mixture (Figure 10c) and has a shape diagnostic of rapid chemical reaction following a reversible electron transfer (an electrochemical EC mechanism). Under these solution conditions, the shape of the current voltage curve for the Mn^{III}/Mn^{IV} process is also similar to that of dyad **6** in Figure 10d.

The cyclic voltammograms of the 1:1 mixture of compounds **1** and **2** is also almost identical to that of **1** when 1 equiv of Cl^- is added to solution in the form of TBACl.[25] These results are consistent with a binding of Cl^- to the electrogenerated Mn(IV) corrole in the mixture.

The fact that the same noncoupled corrole oxidation and re-reduction processes are seen for the monocorrole **1** after addition

dx.doi.org/10.1021/ic102399g |Inorg. Chem. 2011, 50, 3479–3489

of 1.0 equiv of chloride to solution and for **6** (Figure 10d) where the sole source of chloride is the porphyrin part of the molecule suggests a Cl^- ion exchange from the Mn(III) porphyrin to the Mn(IV) corrole as described by the sequence of steps shown in Scheme 4. The first one-electron abstraction involves the corrole unit at E_{pa} = 0.50 V, and this is followed by a rapid exchange of Cl^- from the Mn(III) porphyrin to the electrogenerated Mn(IV) corrole, consistent with a larger binding constant for Cl^- addition to the Mn(IV) corrole than to the Mn(III) porphyrin. The Mn(IV) corrole with ligated Cl^- is harder to reduce (at E_{pc} = 0.17 V for a scan rate of 0.1 V/s, see Figure 10c) than the initially generated Mn(IV) where $E_{1/2}$ = 0.42 V, and this re-reduction is then followed by a reversible Cl^- exchange to give again a dyad with two Mn(III) centers as shown in the scheme.

A similar Cl^- binding reaction can also be observed for all of the dyads, but in the case of **5** two different redox reactions are observed, one involving oxidation of the pyridine-ligated Mn(III) corrole at E_{pa} = 0.53 V followed reoxidation E_{pc} = 0.26 V and the second involving oxidation of the monochloro Mn(III) derivative at $E_{1/2}$ = 0.25 V (see Supporting Information, Figure S4). This is not surprising if one considers the nature of the "O" bridge which generally leads to more rigid and open structures for the dyads, thus allowing for axial coordination of pyridine to the corrole both outside and inside the cavity.[16,51] The reversible chloride ion exchange between the porphyrin and the corrole part of these dyads rapidly occurs after electrooxidation and re-reduction, implying they may be used as anion carriers and mimic some biological activities.

The Cl^- initially bound to the porphyrin is shown as inside the cavity in accordance with the noncoupled Mn^{III}/Mn^{II} reduction of the porphyrin part of the dyads (Figure 10b), and it is also in agreement with the X-ray structure of $(PMes_2CO)Mn_2(OAc)$ (**5OAc**) which shows the anionic acetate ligand inside the cavity and coordinated to both Mn(III) ions (Supporting Information, Figure S3). Although this structure exhibits disorder at the solvent molecule level, the two Mn−O distances could be determined and are equal to 2.070(5) and 2.119(5) Å.[52] Both manganese atoms are slightly shifted out of the four nitrogen planes toward the central acetate ligand (0.231(3) and 0.325(3) Å, respectively).

CONCLUSION

Four cofacial manganese and porphyrin-corrole dyads and their related monomeric corrole and porphyrin were characterized as to their electron transfer properties in PhCN and pyridine containing TBAP and TBAOAc, and the electron transfer site was evaluated as a function of the specific reaction conditions. The electrochemical behavior of the porphyrin-corrole dyads was shown to vary with the solvent (pyridine or PhCN), type of anion added to solution as supporting electrolyte (ClO_4^- or OAc^-), and type of bridge separating the two macrocycles in a face-to-face arrangement. Pyridine and OAc^- both strongly bind to the monoporphyrin **2** in its Mn(III) and Mn(II) oxidation states (see Scheme 1), while pyridine and acetate ion bind to the monocorrole **1** in its Mn(IV), Mn(III), and Mn(II) oxidation states as previously described in the literature.[25] This coordination of OAc^- to both manganese ions within the cavity affects not only the values of half wave potentials but also the reversibility of the electron transfer reactions. This latter effect is most evident in the case of the Mn^{III}/Mn^{II} porphyrin reaction which is reversible for **2** in PhCN or pyridine solutions containing 0.1 M TBAOAc or TBAP but quasi-reversible for the dyads **3**−**6** under the same solution conditions. The acetate ion bound within the cavity of **3**−**6** in PhCN solutions of TBAOAc remains bound to the corrole and porphyrin parts of the molecule after the stepwise addition or abstraction of electrons under the application of a preselected reducing or oxidizing potential, and the overall electron transfer mechanism proceeds as described in Scheme 3. Finally, an intramolecular chloride ion exchange is observed between the porphyrin and the corrole after the Mn(III)/Mn(IV) oxidation of the corrole in the porphyrin-corrole dyads which initially contain $Mn^{III}Cl$ in the porphyrin, and an X-ray structure with an encapsulated acetate ion suggests that chloride, in the neutral dyads **3**−**6**, is also inside the cavity.

ASSOCIATED CONTENT

Supporting Information. One figure showing spectral changes for the monoporphyrin **2** during titration with TBAOAc in PhCN (Figure S1), one figure showing cyclic voltammograms of the monocorrole **1**, monoporphyrin **2**, and porphyrin-corrole dyads **3**−**6** in PhCN containing 0.1 M TBAP (Figure S2), one figure showing the ORTEP drawing of $(PMes_2CO)Mn_2(OAc)$ (**5OAc**) (Figure S3), and one figure showing a cyclic voltammogram of **5** in pyridine containing 0.1 M TBAP (Figure S4). A summary of UV−vis data for all dyads and related monomers under different solvent conditions is given in Table S1. This material is available free of charge via the Internet at http://pubs.acs.org.

AUTHOR INFORMATION

Corresponding Author

*E-mail: kkadish@uh.edu (K.M.K.), jean-michel.barbe@u-bourgogne.fr (J.-M.B.).

ACKNOWLEDGMENT

The support of the Robert A. Welch Foundation (K.M.K., Grant E-680) and the French Ministry of Research (MENRT), CNRS (UMR 5260) and Burgundy Region are gratefully acknowledged. M.E.O thanks the French Ministry of Research for a three year Ph.D. grant.

REFERENCES

(1) Kadish, K. M.; Frémond, L.; Burdet, F.; Barbe, J.-M.; Gros, C. P.; Guilard, R. *J. Inorg. Biochem.* **2006**, *100*, 858–868.

(2) Kadish, K. M.; Frémond, L.; Ou, Z.; Shao, J.; Shi, C.; Anson, F. C.; Burdet, F.; Gros, C. P.; Barbe, J.-M.; Guilard, R. *J. Am. Chem. Soc.* **2005**, *127*, 5625–5631.

(3) Lai, T.; Chan, F.; So, P.; Ma, D.; Wong, K.; Chen, C. *Dalton Trans.* **2006**, 4845–4851.

(4) Liu, Y.; Zhang, H.-J.; Lu, Y.; Cai, Y.-Q.; Liu, X.-L. *Green Chem.* **2007**, *9*, 1114–1119.

(5) Mansuy, D.; Battioni, P. In *Cytochrome P450 Model Systems in Metalloporphyrins in Catalytic Oxidations*; Sheldon, R. A., Ed.; Marcel Dekker: New York, 1994; p 99.

(6) Meunier, B. *Chem. Rev.* **1992**, *92*, 1411–1456.

(7) Rose, E.; Andrioletti, B.; S., Z.; Quelquejeu-Ethève, M. *Chem. Soc. Rev.* **2005**, *34*, 573–583.

(8) Srinivas, K. A.; Kumar, A.; Chauhan, S. M. S. *Chem. Commun.* **2002**, 2456–2457.

(9) Brettar, J.; Gisselbrecht, J.-P.; Gross, M.; Solladié, N. *Chem. Commun.* **2001**, 733–734.

(10) Flamigni, L.; Maria Talarico, A.; Ventura, B.; Rein, R.; Solladié, N. *Chem.—Eur. J.* **2006**, *12*, 701–712.
(11) Guilard, R.; Jérôme, F.; Barbe, J.-M.; Gros, C. P.; Ou, Z.; Shao, J.; Fischer, J.; Weiss, R.; Kadish, K. M. *Inorg. Chem.* **2001**, *40*, 4856–4865.
(12) Kadish, K. M.; Shao, J.; Ou, Z.; Zhan, R.; Burdet, F.; Barbe, J.-M.; Gros, C. P.; Guilard, R. *Inorg. Chem.* **2005**, *44*, 9023–9038.
(13) Rein, R. G.; Gross, M.; Solladié, N. *Chem. Commun.* **2004**, 1992–1993.
(14) Wu, Z.-Q.; Shao, X.-B.; Li, C.; Hou, J.-L.; Wang, K.; Jiang, X.-K.; Li, Z.-T. *J. Am. Chem. Soc.* **2005**, *127*, 17460–17468.
(15) Bolze, F.; Gros, C. P.; Drouin, M.; Espinosa, E.; Harvey, P. D.; Guilard, R. J. *Organomet. Chem.* **2002**, 89–97.
(16) Gros, C. P.; Brisach, F.; Meristoudi, A.; Espinosa, E.; Guilard, R.; Harvey, P. D. *Inorg. Chem.* **2007**, *46*, 125–135.
(17) Harvey, P. D.; Stern, C.; Gros, C. P.; Guilard, R. *Coord. Chem. Rev.* **2007**, *251*, 410–428.
(18) Harvey, P. D.; Stern, C.; Gros, C. P.; Guilard, R. *J. Inorg. Biochem.* **2008**, *102*, 395–405.
(19) Takai, A.; Gros, C. P.; Barbe, J.-M.; Guilard, R.; Fukuzumi, S. *Chem.—Eur. J.* **2009**, *15*, 3110–3122.
(20) Barbe, J.-M.; Canard, G.; Brandès, S.; Guilard, R. *Angew. Chem., Int. Ed.* **2005**, *44*, 3103–3106.
(21) Guilard, R.; Gros, C. P.; Barbe, J.-M.; Espinosa, E.; Jérôme, F.; Tabard, A.; Latour, J.-M.; Shao, J.; Ou, Z.; Kadish, K. M. *Inorg. Chem.* **2004**, *43*, 7441–7455.
(22) Guilard, R.; Jérôme, F.; Gros, C. P.; Barbe, J.-M.; Ou, Z.; Shao, J.; Kadish, K. M. *C.R. Acad. Sci., Ser. IIc: Chim.* **2001**, *4*, 245–254.
(23) Kadish, K. M.; Ou, Z.; Shao, J.; Gros, C. P.; Barbe, J.-M.; Jérôme, F.; Bolze, F.; Burdet, F.; Guilard, R. *Inorg. Chem.* **2002**, *41*, 3990–4005.
(24) Kadish, K. M.; Shao, J.; Ou, Z.; Frémond, L.; Zhan, R.; Burdet, F.; Barbe, J.-M.; Gros, C. P.; Guilard, R. *Inorg. Chem.* **2005**, *44*, 6744–6754.
(25) Shen, J.; El Ojaimi, M.; Chkounda, M.; Gros, C. P.; Barbe, J.-M.; Shao, J.; Guilard, R.; Kadish, K. M. *Inorg. Chem.* **2008**, *47*, 7717–7727.
(26) Arunkumar, C.; Lee, Y.-M.; Lee, J. Y.; Fukuzumi, S.; Nam, W. *Chem.—Eur. J.* **2009**, *15*, 11482–11489.
(27) Fukuzumi, S.; Fujioka, N.; Kotani, H.; Ohkubo, K.; Lee, Y.-M.; Nam, W. *J. Am. Chem. Soc.* **2009**, *131*, 17127–17134.
(28) Golubkov, G.; Gross, Z. *J. Am. Chem. Soc.* **2005**, *127*, 3258–3259.
(29) Kupershmidt, L.; Okun, Z.; Amit, T.; Mandel, S.; Saltsman, I.; Mahammed, A.; Bar-Am, O.; Gross, Z.; Youdim, M. B. H. *J. Neurochem.* **2010**, *113*, 363–373.
(30) Collman, J. P.; Boulatov, R.; Sunderland, C. J.; Shiryaeva, I. M.; Berg, K. E. *J. Am. Chem. Soc.* **2002**, *124*, 10670–10671.
(31) Collman, J. P.; Wagenknecht, P. S.; Hutchison, J. E. *Angew. Chem., Int. Ed.* **1994**, *33*, 1537–1554.
(32) Collman, J. P.; Zeng, L.; Decréau, R. A. *Chem. Commun.* **2003**, 2974–2975.
(33) Ghosh, A.; Steene, E. *J. Inorg. Biochem.* **2002**, *91*, 423–436.
(34) Naruta, Y.; Sasayama, M.-A.; Ichihara, K. *J. Mol. Catal. A: Chem.* **1997**, *117*, 115–121.
(35) Chang, C. J.; Chng, L. L.; Nocera, D. G. *J. Am. Chem. Soc.* **2003**, *125*, 1866–1876.
(36) Chang, C. J.; Deng, Y.; Heyduk, A. F.; Chang, C. K.; Nocera, D. G. *Inorg. Chem.* **2000**, *39*, 959–966.
(37) Chang, C. J.; Deng, Y.; Peng, S.-M.; Lee, G.-H.; Yeh, C.-Y.; Nocera, D. G. *Inorg. Chem.* **2002**, *41*, 3088–3016.
(38) Lin, X. Q.; Kadish, K. M. *Anal. Chem.* **1985**, *57*, 1498–1501.
(39) Barbe, J.-M.; Burdet, F.; Espinosa, E.; Guilard, R. *Eur. J. Inorg. Chem.* **2005**, 1032–1041.
(40) El Ojaimi, M.; Gros, C. P.; Barbe, J.-M. *Eur. J. Org. Chem.* **2008**, *7*, 1181–1186.
(41) Kadish, K. M.; Frémond, L.; Shen, J.; Chen, P.; Ohkubo, K.; Fukuzumi, S.; El Ojaimi, M.; Gros, C. P.; Barbe, J.-M.; Guilard, R. *Inorg. Chem.* **2009**, *48*, 2571–2582.
(42) Boucher, L. J. *J. Am. Chem. Soc.* **1970**, *92*, 2725–2730.
(43) Fryxelius, J.; Eilers, G.; Feyziyev, Y.; Magnuson, A.; Sun, L.; Lomoth, R. *J. Porphyrins Phthalocyanines* **2005**, *9*, 379–386.
(44) Krzystek, J.; Pardi, L. A.; Brunel, L.-C.; Goldberg, D. P.; Hoffman, B. M.; Licoccia, S.; Telser, J. *Spectrochim. Acta, Part A* **2002**, *58A*, 1113–1127.
(45) Krzystek, J.; Telser, J.; Hoffman, B. M.; Brunel, L.-C.; Licoccia, S. *J. Am. Chem. Soc.* **2001**, *123*, 7890–7897.
(46) Guilard, R.; Burdet, F.; Barbe, J.-M.; Gros, C. P.; Espinosa, E.; Shao, J.; Ou, Z.; Zhan, R.; Kadish, K. M. *Inorg. Chem.* **2005**, *44*, 3972–3983.
(47) Camenzind, M. J.; Hollander, F. J.; Hill, C. L. *Inorg. Chem.* **1983**, *22*, 3776–3784.
(48) Mu, X.; Schultz, F. *Inorg. Chem.* **1992**, *31*, 3351–3357.
(49) Sanders, J. K. M.; Bampos, N.; Clyde-Watson, Z.; Darling, S. L.; Hawley, J. C.; Kim, H.-J.; Mak, C. C.; Webb, S. J. In *The Porphyrin Handbook*; Kadish, K. M., Smith, K. M., Guilard, R., Eds.; Academic Press: San Diego, 2000; Vol. 3, pp 1−48.
(50) Ruhlmann, L.; Zimmermann, J.; Fudickar, W.; Siggel, U.; Fuhrhop, J. H. *J. Electroanal. Chem.* **2001**, *503*, 1–14.
(51) Gros, C. P.; Aly, S. M.; El Ojaimi, M.; Barbe, J. M.; Brisach, F.; Abd-El-Aziz, A. S.; Guilard, R.; Harvey, P. D. *J. Porphyrins Phthalocyanines* **2007**, *11*, 244–257.
(52) Paolesse, R.; Di Natale, C.; Macagnano, A.; Sagone, F.; Scarselli, M. A.; Chiaradia, P.; Troitsky, V. T.; Berzina, T. S.; D'Amico, A. *Langmuir* **1999**, *15*, 1268.